



Article

# Promotional Effect of Pt-Doping on the Catalytic Performance of Pt–CeO<sub>2</sub> Catalyst for CO Oxidation

Angran Jiang<sup>1</sup>, Zhibo Ren<sup>2</sup> , Yaqi Qu<sup>1</sup> , Yanjun Zhang<sup>1</sup> and Jianwei Li<sup>1,\*</sup>

<sup>1</sup> State Key Laboratory of Chemical Resources Engineering, Beijing University of Chemical Technology, Beijing 100029, China; jiangangran@163.com (A.J.); quyqcatalysis@gmail.com (Y.Q.); zhangyjbuict@126.com (Y.Z.)

<sup>2</sup> Huaneng Clean Energy Research Institute, Beijing 102209, China; zbrenbuict@gmail.com

\* Correspondence: lijw@mail.buct.edu.cn; Tel.: +86-010-644-36787

**Abstract:** Growing interest in the development of a hydrogen economy means that CO oxidation is increasingly important for upgrading H<sub>2</sub>-rich fuel gas streams for fuel cells. CeO<sub>2</sub>-supported catalysts are the most promising candidates for the catalytic oxidation of CO because of their high activity. In the present work, DFT+U calculations were performed to investigate the stability and CO oxidation reactivity of Pt<sub>n</sub> (*n* = 1–4) clusters supported on CeO<sub>2</sub>(111) (Pt/CeO<sub>2</sub>) and Pt-doped CeO<sub>2</sub>(111) (Pt/(Pt–Ce)O<sub>2</sub>) surfaces. The Pt clusters showed similar nucleation behavior on both CeO<sub>2</sub> and (Pt–Ce)O<sub>2</sub> surfaces. Further, the formation of oxygen vacancies (O<sub>v</sub>) was facilitated because of surface charge depletion caused by the dopant Pt. Our DFT results suggest that the interfacial O<sub>v</sub> plays an important role in the CO oxidation reaction cycle, and the calculated energy barrier for the CO oxidation reaction on the Pt/(Pt–Ce)O<sub>2</sub> surface is approximately 0.43 eV lower than that on the surface of the undoped catalyst, suggesting enhanced CO oxidation reactivity. Therefore, the chemical modification of the CeO<sub>2</sub> support via doping is an effective strategy for improving the catalytic performance of Pt/CeO<sub>2</sub>.



**Citation:** Jiang, A.; Ren, Z.; Qu, Y.; Zhang, Y.; Li, J. Promotional Effect of Pt-Doping on the Catalytic Performance of Pt–CeO<sub>2</sub> Catalyst for CO Oxidation. *Catalysts* **2022**, *12*, 529. <https://doi.org/10.3390/catal12050529>

Academic Editor: Leonarda Francesca Liotta

Received: 13 March 2022

Accepted: 27 April 2022

Published: 9 May 2022

**Publisher's Note:** MDPI stays neutral with regard to jurisdictional claims in published maps and institutional affiliations.



**Copyright:** © 2022 by the authors. Licensee MDPI, Basel, Switzerland. This article is an open access article distributed under the terms and conditions of the Creative Commons Attribution (CC BY) license (<https://creativecommons.org/licenses/by/4.0/>).

**Keywords:** CO oxidation; Pt/CeO<sub>2</sub> catalysts; density functional theory

## 1. Introduction

Cerium oxide (CeO<sub>2</sub>)-based catalysts have been widely used in many catalytic processes, such as the water–gas shift reaction [1], methanol synthesis [2], and CO oxidation [3]. CO oxidation is becoming increasingly important to remove CO from reformat streams to obtain fuel-cell-grade hydrogen [4,5]. Pt-group metals supported on reducible oxides, such as TiO<sub>2</sub> [6] and CeO<sub>2</sub>, are regarded as promising low-temperature CO removal catalysts [7]. Thus, CeO<sub>2</sub>-supported Pt catalysts and their role in CO oxidation have drawn extensive interest both experimentally and theoretically. Boronin et al. synthesized Pt/CeO<sub>2</sub> catalysts having a range of Pt loadings, and the 8 and 20 wt% Pt catalysts were found to convert 60% and 90% of CO below 0 °C because of the synergistic reaction between ionic platinum and nanostructured ceria [8]. The superior activity of high Pt loading catalyst was attributed to a high concentration of Pt ions, with a fraction of the ionic Pt content aggregated into clusters. Liu et al. investigated CO oxidation on CeO<sub>2</sub>(111)-supported Pd-based bimetallic nanorods using density functional theory (DFT) and found that the formation of a bimetallic system having complementary chemical properties was effective for tuning the catalytic activity [9]. In particular, the superior activity of CeO<sub>2</sub>-supported catalysts lies in their high oxygen storage capacities [10] and strong metal–support interactions [11], which not only lowers the oxygen vacancy formation energy (*E*<sub>vac</sub>) on the CeO<sub>2</sub> surface but also facilitates CO oxidation via the Mars–Van Krevelen (M-VK) mechanism [12]. On the other hand, the metal–support interaction can stabilize the metal clusters on the surface of the support [13], which results in excellent anti-sintering performance under reactive conditions.

As previously reported, small Pt clusters supported on the CeO<sub>2</sub> surface provide active sites for CO oxidation and show higher activity than atomically supported Pt atoms [14,15]. In particular, the surface oxygen atoms at the Pt/CeO<sub>2</sub> interface play an extremely important role during the CO oxidation process. Lu et al. found that CO adsorbs strongly on Pt clusters, whereas the highly active lattice oxygen sites near the Pt clusters overcome the strong bonds of CO adsorbed on the Pt cluster [16]. Many attempts have been made to enhance the activity of the metal–oxide interface, for example, by adjusting the size of metal clusters and creating surface oxide defects near the clusters [17]. Recently, computational evidence has suggested that the doping of the CeO<sub>2</sub> support is a promising way to accelerate CO oxidation at the metal–support interface [18].

The doping of the CeO<sub>2</sub> surface with metals is reported to reduce the oxygen vacancy formation energy of nearby surface oxygen atoms significantly [19]. The oxygen vacancy formation energy varies with the position of the dopant in the periodic table [20]—when low-valence metals are doped on the surface of CeO<sub>2</sub>, fewer electrons are transferred to the surrounding oxygen atoms than from Ce<sup>4+</sup>, which results in electron depletion in the CeO<sub>2</sub> support. This further weakens the bonds between electrophilic oxygen atoms and the surface atoms and reduces the oxygen vacancy formation energy,  $E_{\text{vac}}$  [21]. Hu et al. [22] studied the effects that reduce the oxygen vacancy formation energy on the insertion of metal atoms on the surface of CeO<sub>2</sub> and found that the doping of the CeO<sub>2</sub> support with low-valence metals, such as Y and La, can reduce the oxygen vacancy formation energy in the long range. In contrast, the high valence dopants, such as Pt and Zr, just create a weak electron deficit in the CeO<sub>2</sub>(111) surface, and the oxygen vacancy formation energy is only reduced near the surface [23].

In the present work, the influence of doping Pt/CeO<sub>2</sub> catalyst with a heterometal (Pt) was investigated using DFT calculations. Firstly, we identified the most stable Pt-doped CeO<sub>2</sub>(111) surface structure. Secondly, the adsorption and nucleation of the supported Pt<sub>*n*</sub> (*n* = 1–4) clusters were explored. Finally, the structural changes and energies of oxygen vacancy formation and CO oxidation on the Pt-support interface were studied to gain insights into the catalytic activity of the small CeO<sub>2</sub>-supported Pt clusters.

## 2. Results

### 2.1. Structures of Pristine and Pt-doped CeO<sub>2</sub>(111) Surface

A model of the CeO<sub>2</sub>(111) surface doped with Pt was obtained by replacing a single surface Ce<sup>4+</sup> ion with a Pt<sup>4+</sup> ion. Two stable structures were then found, namely (Pt–Ce)O<sub>2</sub>\_I, in which the dopant Pt atom has a square planar structure, and (Pt–Ce)O<sub>2</sub>\_II, in which the Pt atom has a regular octahedral structure (Figure 1); these structures are similar to those reported by Su et al. [24]. In fact, the total energy of the (Pt–Ce)O<sub>2</sub>\_II structure is 0.54 eV lower than that of the (Pt–Ce)O<sub>2</sub>\_I structure, indicating the (Pt–Ce)O<sub>2</sub>\_II structure is thermodynamically more favorable [25]. The radii of the Pt<sup>4+</sup> (0.77 Å) is a little smaller than that of the Ce<sup>4+</sup> (0.97 Å) [12]; thus, the dopant Pt is more inclined to form an octahedral structure. Therefore, the (Pt–Ce)O<sub>2</sub>\_II model structure was used in the following studies and is denoted as (Pt–Ce)O<sub>2</sub> in subsequent sections.

### 2.2. Stability of Pt<sub>*n*</sub> Clusters

Next, in the computational model, Pt<sub>1–4</sub> clusters were loaded onto the perfect CeO<sub>2</sub> and (Pt–Ce)O<sub>2</sub> surfaces to enable the investigation of the interaction between Pt clusters and different support surfaces. The doped Pt cations were supposed to be a nucleation center for supported Pt nanoparticles and Pt clusters formed at positions where Pt<sup>2+</sup> is doped into the framework. Once acting as a nucleation center for supported metal nanoparticles, dopants such as Ni, Pd, Pt, and Rh cannot activate lattice O atoms [24]. Therefore, Pt clusters were deposited on the neighboring site of Pt dopant to study its short range doping effect as in the previous study [18]. The most stable adsorption structures in terms of thermodynamics for each composition and adsorption energies are shown in Figure 2. As shown, a single Pt atom preferentially adsorbs close to O-hollow site between two O anions

on both  $\text{CeO}_2(111)$  and the  $(\text{Pt}-\text{Ce})\text{O}_2$  surfaces, having adsorption energies of  $-2.84$  and  $-3.06$  eV, respectively. Consistent with the results of previous studies, the adsorption of the  $\text{Pt}_2$  dimer on the O-O bridge site is more stable than that of an isolated Pt atom on both support surfaces [26]. The adsorption energy of  $\text{Pt}_2$  on clean  $\text{CeO}_2(111)$  is  $-2.97$  eV, which is larger than that on the  $(\text{Pt}-\text{Ce})\text{O}_2$  surface. For  $\text{Pt}_3$  on both surfaces, a flat triangular Pt cluster in which each Pt atom forms a close interaction with the surface O atoms of  $\text{CeO}_2$  is the most relatively stable structure. However, in the triangular structure, one of the Pt atoms forms a shorter Pt-O bond,  $1.84$  Å (the others are  $1.92$  and  $1.95$  Å). The adsorption energies of the supported  $\text{Pt}_3$  cluster on both surfaces are lower (by about 1 eV) than that of the  $\text{Pt}_2$  cluster adsorbed on the same surfaces. When we modeled the adsorption of four Pt atoms on both surfaces, a tetrahedral configuration was formed; in this structure on both surfaces, three Pt atoms interact with the surfaces through Pt-O bonds, and the remaining Pt atom is located at the top vertex pointing away from the support surface.

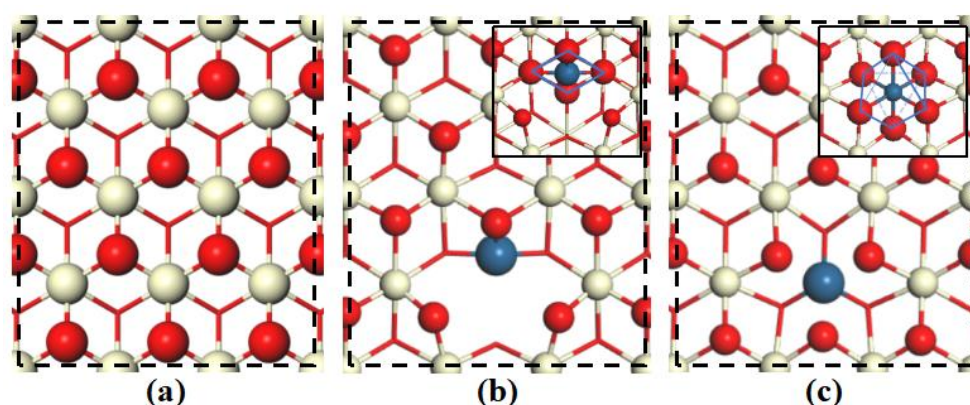


**Figure 1.** Top views of the optimized configurations of the support surface: (a)  $\text{CeO}_2(111)$ , (b)  $(\text{Pt}-\text{Ce})\text{O}_2\text{_I}$ , and (c)  $(\text{Pt}-\text{Ce})\text{O}_2\text{_II}$ . The inset in (b) and (c) show the detailed configuration of the doped Pt. Ce (pale yellow), O (red), and Pt (cyan).

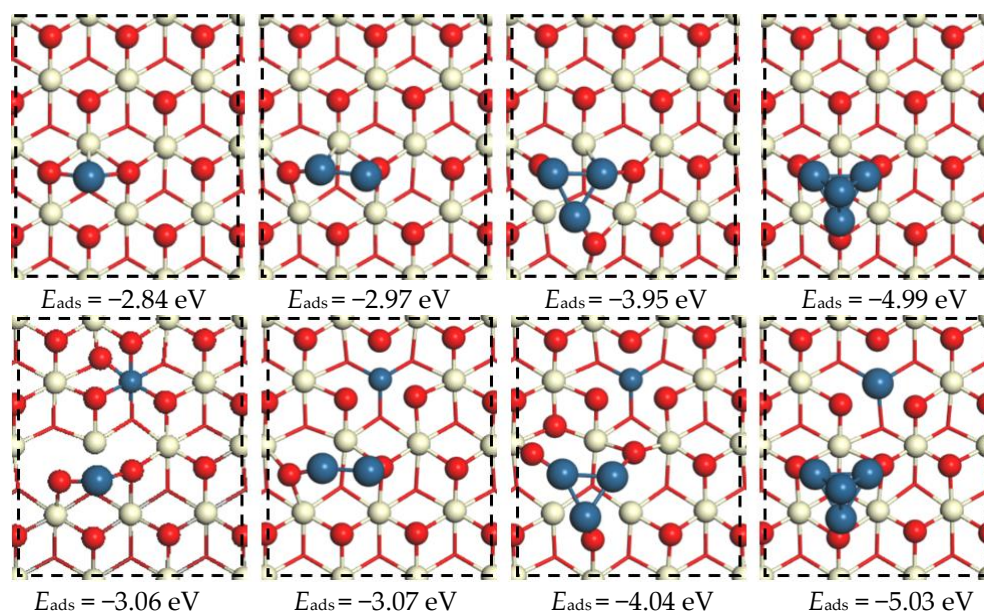


**Figure 2.** Top views of the optimized configurations of  $\text{Pt}_n$  clusters on the  $\text{CeO}_2$  surface (up) and  $(\text{Pt}-\text{Ce})\text{O}_2$  surface (down).



The DFT calculations show that the  $Pt_n$  ( $n = 1-4$ ) clusters adsorbed on the  $CeO_2(111)$  and  $(Pt-Ce)O_2$  surfaces have similar adsorption energies, but that on the doped surface is slightly lower than that on the pristine surface. In addition, as the number of Pt atoms in the  $Pt_n$  cluster increases, the difference between the adsorption energies on the  $CeO_2(111)$  and  $(Pt-Ce)O_2$  surfaces gradually decreases. These results suggest that the metal dopants do not significantly affect the stability of the supported Pt clusters.

As shown in Figure 3, the nucleation energy with respect to the size of the  $Pt_n$  ( $n = 1-4$ ) clusters adsorbed on both  $CeO_2$  and  $(Pt-Ce)O_2$  surfaces show similar trends. The negative nucleation energy indicates an exothermic process, and the cluster tends to aggregate. As seen in the Figure 3, Pt clusters supported on  $CeO_2(111)$  surface showed an aggregation trend with negative nucleation energy, which has been observed in previous study on  $Cu/CeO_2$  system [26]. Furthermore, the nucleation energy of the  $Pt_n$  ( $n = 1-4$ ) clusters adsorbed on  $CeO_2(111)$  surface is slightly higher than that of the  $Pt_n$  ( $n = 1-4$ ) clusters adsorbed on the  $(Pt-Ce)O_2$  surface, and, at  $n = 4$ , the difference reaches the maximum, 0.43 eV. Therefore, the dopant of Pt has no obvious effect on the nucleation of clusters.  $Pt_4$  is the smallest three-dimensional cluster and is also a typical model in theoretical calculations, so the  $Pt_4/CeO_2$  and  $Pt_4/(Pt-Ce)O_2$  models were used for subsequent calculations.

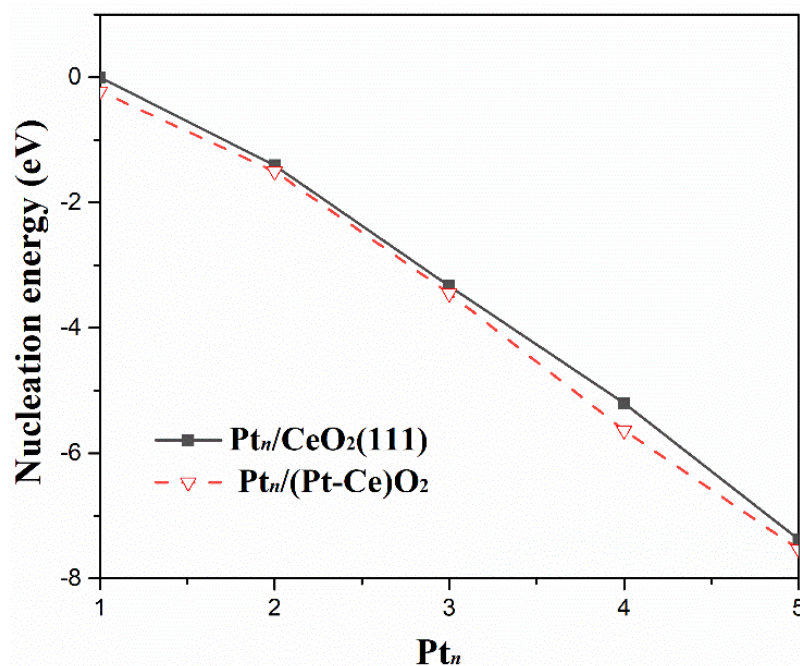


**Figure 3.** Nucleation energies as a function of the number of Pt atoms in the  $Pt_n$  cluster on  $CeO_2$  and  $(Pt-Ce)O_2$  surface.

### 2.3. Oxygen Vacancy Formation

To explore the change in the activity of the surface oxygen atoms before and after Pt atom doping, the oxygen vacancy formation energies on the  $Pt_4/CeO_2$  and  $Pt_4/(Pt-Ce)O_2$  interfaces were calculated. The position of the surface vacancy is indicated by way of a dotted circle in Figure 4, and those formation energies on the  $Pt_4/(Pt-Ce)O_2$  and  $Pt_4/CeO_2$  surfaces were calculated to be 0.37 and 2.19 eV, respectively. Thus, the insertion of Pt atoms facilitates the formation of oxygen vacancies at the metal-support interface and enhances the activity of the surface oxygen atoms.

Next, Bader charge analysis of both the  $Pt_4/CeO_2$  and  $Pt_4/(Pt-Ce)O_2$  surfaces was performed to explore the differences in the charge distribution caused by doping with Pt. A detailed charge distribution diagram of both surfaces loaded with a single  $Pt_4$  cluster is shown in Figure 4. For the  $Pt_4/(Pt-Ce)O_2$  system, the oxidation state of the doped Pt atoms is  $+1.50e$ , whereas that of the Ce atoms at the same position without the Pt dopant is  $+2.41e$ . This is because the amount of positive charge carried by the doped Pt atoms is significantly

less than that of the subsurface Ce atoms replaced by Pt atoms. On the insertion of a Pt atom, the surface oxygen atoms associated with it (indicated by a dotted circle) have an oxidation state of  $-1.01e$ , whereas the other surface oxygen atoms have an oxidation state between  $-1.10e$  and  $-1.20e$ . Therefore, Pt doping results in charge redistribution at the  $\text{CeO}_2$  surface. The total Bader charge of  $\text{Pt}_1$ ,  $\text{Pt}_2$ ,  $\text{Pt}_3$ , and  $\text{Pt}_4$  supported on  $\text{CeO}_2$  surface is  $0.05e$ ,  $0.02e$ ,  $0.03e$ , and  $0.05e$ , respectively. After the Pt doping, it can be observed that the total Bader charge of  $\text{Pt}_n$  ( $n = 1-4$ ) will increase to  $0.19e$ ,  $0.10e$ ,  $0.12e$ , and  $0.15e$ , respectively. In particular, the surface charge depletion caused by doping with Pt reduces the charge of the nearby surface oxygen atoms, which makes detachment from the surface easier, thus resulting in the formation of oxygen vacancies.

It can be observed from the results of Bader charge analysis and adsorption energy of both  $\text{Pt}_4/\text{CeO}_2$  and  $\text{Pt}_4/(\text{Pt}-\text{Ce})\text{O}_2$  surfaces that Pt clusters near the doped site have slightly more positive charges and stronger adsorption energies. The charge depletion caused by Pt dopant enhances the interaction between Pt cluster and support surface. As mentioned in Liu's work [27], the adsorption energy of CO varies with clusters' oxidation state. Therefore, the dopant of Pt increases the oxidation state of the Pt clusters on the nearby surface, thereby weakening the CO adsorption.

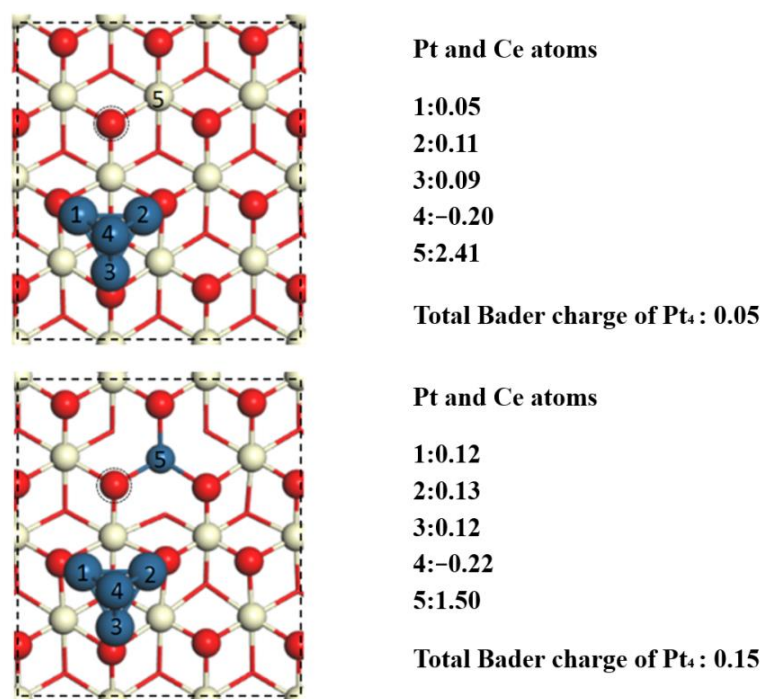


**Figure 4.** Bader charge analysis of (a)  $\text{Pt}_4/\text{CeO}_2$  and (b)  $\text{Pt}_4/(\text{Pt}-\text{Ce})\text{O}_2$ . The dotted circle represents the removed O atom to form oxygen vacancy.

#### 2.4. CO Oxidation on the $\text{Pt}_4/(\text{Pt}-\text{Ce})\text{O}_2$ and $\text{Pt}_4/\text{CeO}_2$ Surfaces

The oxygen atom activity, which is affected by the charge transfer from the Pt dopant atom, plays an important role in improving the catalytic CO oxidation activity of the Pt clusters adsorbed nearby on the surface. To explore this, the energies of each elementary step in the CO oxidation reaction occurring on the  $\text{Pt}_4/\text{CeO}_2$  and  $\text{Pt}_4/(\text{Pt}-\text{Ce})\text{O}_2$  surfaces were calculated based on the M-VK mechanism. The corresponding models and energies of the CO oxidation reaction are shown in Figures 5 and 6, respectively.

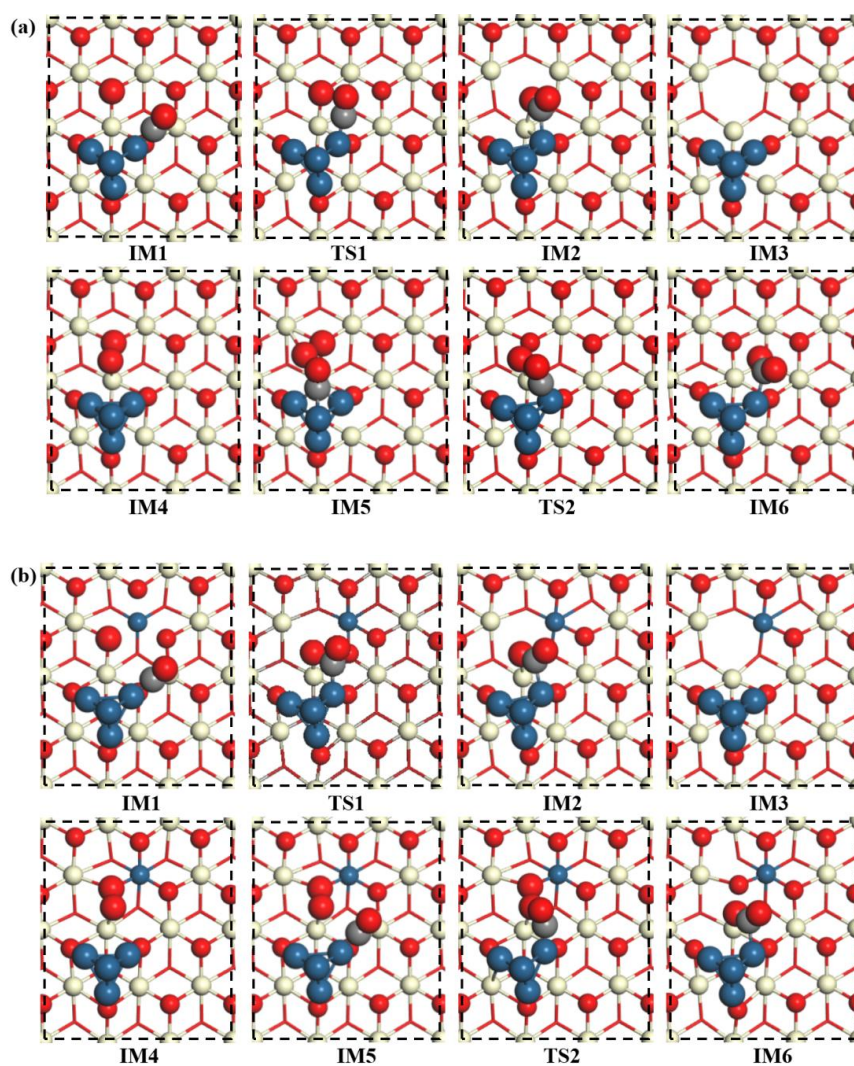


**Figure 5.** Top view of CO oxidation on the (a)  $\text{Pt}_4/\text{CeO}_2$  and (b)  $\text{Pt}_4/(\text{Pt}-\text{Ce})\text{O}_2$  surfaces. (IM: intermediate; TS: transition state; FS: final state).

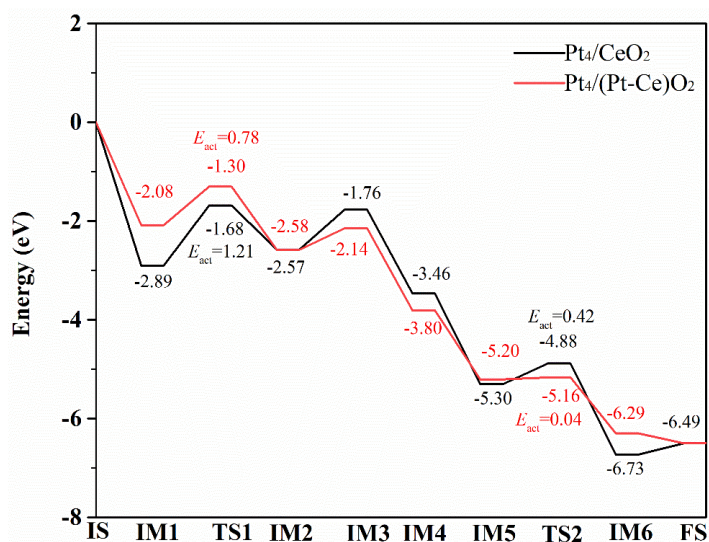


**Figure 6.** Calculated energy profiles for CO oxidation on the  $\text{Pt}_4/\text{CeO}_2$  and  $\text{Pt}_4/(\text{Pt}-\text{Ce})\text{O}_2$  surfaces. The activation energy ( $E_{\text{act}}$ ) is the energy of the transition state relative to the previous stage.

In the CO oxidation process at the Pt<sub>4</sub>/CeO<sub>2</sub> interface, CO is first adsorbed with an adsorption energy of 2.89 eV near the Pt atoms at the Pt–support interface. The lengths of the Pt-C and C-O bonds in the adsorbed CO were calculated to be 1.84 and 1.16 Å, respectively (IM1). In the next step, CO combines with oxygen atoms on the support surface to form a triangular reaction intermediate (denoted TRI, IM2) in an endothermic process, having an energy of 0.32 eV. Here, the Pt-C bond length in IM2 lengthens to 2.06 Å.

Next, the oxygen atom at the active site is attracted by the C atom in CO to form a C-O bond having a length of 1.31 Å, and one of the O-Ce bonds formed with this oxygen atom is broken, and the length of the other Ce-O bond is elongated to 2.51 Å. The decomposition of the first TRI structure to produce a gaseous CO<sub>2</sub> molecule requires 0.89 eV, and this process can lead to the formation of an oxygen vacancy (IM3).

In the next step, O<sub>2</sub> is adsorbed on the surface with an adsorption energy of −1.70 eV and fills the oxygen vacancy (IM4). The length of the elongated O-O length in the O<sub>2</sub> molecule is 1.46 Å. Further, a second CO molecule is adsorbed on the Pt atom with an adsorption energy of 1.83 eV, and the C atom of the CO molecule forms three Pt-C bonds, whose bond lengths range from 2.05 to 2.06 Å (IM5). Subsequently, the adsorbed CO combines with the O<sub>2</sub> adsorbed on the oxygen vacancy to form a second TRI structure (IM6). In this process, the O-Ce bond of adsorbed O<sub>2</sub> breaks, as does the O-O bond in molecular oxygen, and two of the three Pt-C bonds formed with the C atom of adsorbed CO break; the remaining Pt-C bond is thus shortened to 2.01 Å. The shift from IM5 to IM6 is strongly exothermic, having an energy of −1.43 eV. Finally, the TRI structure decomposes to form a second molecule of CO<sub>2</sub> with an energy change of 0.23 eV (FS), resulting in the catalyst regaining its original structure.

The energy profile of the reaction shows that the formation of the TRI structure is the key step of the reaction. One of the reasons for this is the strong adsorption of CO on the Pt atoms, and the other is the lack of high activity of oxygen atoms at the interface of Pt<sub>4</sub>/CeO<sub>2</sub>. Both of these factors lead to a higher reaction energy barrier, about 1.21 eV.

For the CO oxidation reaction on the surface of Pt<sub>4</sub>/(Pt–Ce)O<sub>2</sub>, the first molecule of CO is adsorbed on the Pt atom close to the dopant Pt atom. This process leads to an energy change of −2.08 eV, suggesting the weaker adsorption of CO on the Pt cluster as a result of the insertion of a Pt atom on the nearby surface. In this structure, the C-O bond length is 1.16 Å, and the Pt-C bond length is 1.85 Å. Clearly, the bond length of the adsorbed CO is longer than that of the adsorbed CO at the Pt<sub>4</sub>/CeO<sub>2</sub> interface. Next, IM2 is formed by the adsorbed CO moving towards and combining with a surface O atom. In IM2, the Pt-C bond length is 2.07 Å, and a C-O bond between the oxygen atom at the active site and the C atom of the adsorbed CO is formed at the Pt<sub>4</sub>/(Pt–Ce)O<sub>2</sub> interface, having a bond length of 1.28 Å. In addition, one of the O-Ce bonds between the reactive oxygen atom and the two Ce atoms is also broken, as for the process occurring at the Pt<sub>4</sub>/CeO<sub>2</sub> interface. However, the Ce-O bond length of the other is 2.46 Å, which is slightly shorter than the 2.51 Å bond at the Pt<sub>4</sub>/CeO<sub>2</sub> interface. The transition from IM1 to IM2 is an exothermic process, having an energy change of −0.5 eV, and the energy barrier is only 0.78 eV. The decomposition of TRI in IM3 adsorbs 0.44 eV energy, making it the rate-determining step. This energy is much less than that adsorbed in the same process on the Pt<sub>4</sub>/CeO<sub>2</sub> surface (0.9 eV). In IM4, O<sub>2</sub> is adsorbed on the oxygen vacancy between Pt<sub>4</sub> and the support, yielding an O-O bond length of 1.43 Å and an adsorption energy of −1.66 eV; further, when CO is adsorbed on the Pt<sub>4</sub> clusters in IM5 with an adsorption energy of 1.40 eV, the C-O bond length is 1.20 Å. In the second TRI structure, the O-O bond in the adsorbed O<sub>2</sub> molecule is broken, and O atom simultaneously bonds with the C atom of the adsorbed CO and a surface Ce atom, forming bonds having lengths of 2.43 and 1.26 Å, respectively. In this structure, the Pt-C bond length changes to 2.08 Å. Notably, the formation of the TRI structure releases 1.09 eV of energy and has a low energy barrier of 0.04 eV. The key step of the reaction is the decomposition of IM3, which is endothermic by 0.44 eV. The relatively weaker adsorption of CO and more active surface oxygen atoms can be attributed to the lower energy barrier of the reaction.



A comparison of the energy profiles of the CO oxidation reaction over the Pt<sub>4</sub>/CeO<sub>2</sub> and Pt<sub>4</sub>/(Pt–Ce)O<sub>2</sub> surfaces shows that the lattice oxygen atom activity is significantly enhanced, but the adsorption of CO is significantly weakened when the CeO<sub>2</sub> surface is doped with Pt. Crucially, the insertion of Pt atoms reduces the energy of CO oxidation, that is, the rate-limiting step of the reaction, and  $E_{\text{vac}}$  decreases from 1.21 to 0.78 eV.

### 3. Computation Details

All spin-polarized periodic DFT calculations were performed using the Vienna Ab initio Simulation Package (VASP 5.4) [28,29]. The electron exchange and correlation were treated within the generalized gradient approximation (GGA) using the Perdew–Burke–Ernzerhof (PBE) functional [30]. The core electrons of all the atoms were described by the projector-augmented wave (PAW) pseudopotential with a cut-off energy of 450 eV [31]. A spin-polarized DFT+U calculations with a value of  $U = 4.5$  eV was used for the description of Ce 4f states [32]. The lattice parameter for bulk CeO<sub>2</sub> is set to our previously calculated DFT+U value (5.44 Å) [33]. The CeO<sub>2</sub>(111) surface was modeled containing a (4 × 3) unit cell with three Ce–O–Ce layers and the Pt doped surface was constructed by substituting a surface Ce atom with a Pt atom. During geometry optimization, the bottom Ce–O–Ce layer were fixed, while the other layers and adsorbates were fully relaxed. The k-points sampling was generated by the Monkhorst Pack procedure with a (4 × 4 × 1) mesh and a 15 Å vacuum region was introduced to eliminate the interaction between Z-axis atoms. The electronic self-consistent field was converged to 10<sup>−5</sup> eV and the forces on all atoms were converged to less than 0.02 eV / Å. Bader charge provides a good approximation to the total electronic charge of atoms in computational system. Bader analysis was performed with the code developed by Henkelman et al. to quantify charge transfer between atoms [34]. The adsorption energy ( $E_{\text{ads}}$ ) of Pt<sub>*n*</sub> clusters was calculated by:

$$E_{\text{ads}} = E(\text{Pt}_n/\text{Slab}) - E(\text{Slab}) - E(\text{Pt}_n) \quad (1)$$

The nucleation energy ( $E_{\text{nuc}}$ ) of Pt<sub>*n*</sub> ( $n = 1-4$ ) clusters was calculated to quantify the nucleation processes of small Pt<sub>*n*</sub> cluster on the support surface.

$$E_{\text{nuc}} = E(\text{Pt}_n/\text{Slab}) - nE(\text{Pt}_1/\text{Slab}) + (n-1)E(\text{Slab}) \quad (2)$$

The TS of surface reactions were searched using the climbing image nudged elastic band (CI-NEB) method [35] and the maximum force was converged to less than 0.05 eV / Å. The stretching frequencies were analyzed to characterize a transition state with single imaginary frequency along the reaction coordinate. The activation energy was determined as the energy difference between the corresponding TS and initial states (IS) and the reaction energy was defined as the corresponding FS and IS energy difference.

### 4. Conclusions

In this study, using DFT calculations, we investigated the effect of dopant Pt atoms on (1) the energy of Pt<sub>*n*</sub> ( $n = 1-4$ ) clusters with respect to size on pristine and doped CeO<sub>2</sub>(111) surfaces, (2) the activity of the surface O atoms, and (3) the CO oxidation cycle at the Pt–CeO<sub>2</sub> interface. By calculating the nucleation energies of the Pt clusters on the undoped and Pt-doped surfaces, we found that the dopant had a negligible effect on the stability of the Pt clusters with respect to size. In addition, we found that the doping of metal atoms can enhance the surface oxygen atom activity via charge depletion on the oxide surface, thus lowering the oxygen formation energy. The dopant Pt atoms facilitate the key step in CO oxidation at the metal–substrate interface by lowering the energy required for the formation of TRI, which subsequently yields CO<sub>2</sub>. Moreover, the energy barrier for the reaction of CO with surface oxygen atoms is reduced, thereby improving the reaction activity. This study also illustrates that the combination of Pt dopant atoms and Pt clusters on the dopant surface can significantly improve the catalytic performance. Our theoretical



computation results provide important insights for developing thermally stable and active Pt/CeO<sub>2</sub> catalysts for CO oxidation.

**Author Contributions:** Conceptualization, A.J. and Z.R.; methodology, A.J. and Z.R.; software, A.J.; validation, A.J.; formal analysis, A.J. and Z.R.; investigation, A.J. and Z.R.; resources, J.L; data curation, A.J.; writing—original draft preparation, A.J.; writing—review and editing, Y.Q. and Y.Z.; supervision, J.L. All authors have read and agreed to the published version of the manuscript.

**Funding:** This research received no external funding.

**Data Availability Statement:** Not applicable.

**Acknowledgments:** Not applicable.

**Conflicts of Interest:** The authors declare no conflict of interest.

## References

1. Maciel, C.G.; de Freitas Silva, T.; Assaf, E.M.; Assaf, J.M. Hydrogen production and purification from the water-gas shift reaction on CuO/CeO<sub>2</sub>-TiO<sub>2</sub> catalysts. *Appl. Energy* **2013**, *112*, 52–59. [[CrossRef](#)]
2. Zhu, J.; Su, Y.; Chai, J.; Muravev, V.; Kosinov, N.; Hensen, E.J.M. Mechanism and nature of active sites for methanol synthesis from CO/CO<sub>2</sub> on Cu/CeO<sub>2</sub>. *ACS Catal.* **2020**, *10*, 11532–11544. [[CrossRef](#)]
3. Polychronopoulou, K.; Alkhoori, A.A.; Efstathiou, A.M.; Jaoude, M.A.; Damaskinos, C.M.; Baker, M.A.; Almutawa, A.; Anjum, D.H.; Vasiliades, M.A.; Belabbes, A.; et al. Design aspects of doped CeO<sub>2</sub> for low-temperature catalytic CO oxidation: Transient kinetics and DFT approach. *ACS Appl. Mater. Interfaces* **2021**, *13*, 22391–22415. [[CrossRef](#)] [[PubMed](#)]
4. Rodriguez, J.A.; Grinter, D.C.; Liu, Z.; Palomino, R.M.; Senanayake, S.D. Ceria-based model catalysts: Fundamental studies on the importance of the metal-ceria interface in CO oxidation, the water-gas shift, CO<sub>2</sub> hydrogenation, and methane and alcohol reforming. *Chem. Soc. Rev.* **2017**, *46*, 1824–1841. [[CrossRef](#)] [[PubMed](#)]
5. Aneghi, E.; De Leitenburg, C.; Trovarelli, A. On the role of lattice/surface oxygen in ceria-zirconia catalysts for diesel soot combustion. *Catal. Today* **2012**, *181*, 108–115. [[CrossRef](#)]
6. Li, N.; Chen, Q.-Y.; Luo, L.-F.; Huang, W.-X.; Luo, M.-F.; Hu, G.S.; Lu, J.-Q. Kinetic study and the effect of particle size on low temperature CO oxidation over Pt/TiO<sub>2</sub> catalysts. *Appl. Catal. B Environ.* **2013**, *142–143*, 523–532. [[CrossRef](#)]
7. Slavinskaya, E.M.; Gulyaev, R.V.; Zadesenets, A.V.; Stonkus, O.A.; Zaikovskii, V.I.; Shubin, Y.V.; Korenev, S.V.; Boronin, A.I. Low-temperature CO oxidation by Pd/CeO<sub>2</sub> catalysts synthesized using the coprecipitation method. *Appl. Catal. B Environ.* **2015**, *166–167*, 91–103. [[CrossRef](#)]
8. Boronin, A.I.; Slavinskaya, E.M.; Figueroba, A.; Stadnichenko, A.I.; Kardash, T.Y.; Stonkus, O.A.; Fedorova, E.A.; Muravev, V.V.; Svetlichnyi, V.A.; Bruix, A.; et al. CO oxidation activity of Pt/CeO<sub>2</sub> catalysts below 0 °C: Platinum loading effects. *Appl. Catal. B Environ.* **2021**, *286*, 119931. [[CrossRef](#)]
9. Liu, B.; Zhao, Z.; Henkelman, G.; Song, W. Computational design of a CeO<sub>2</sub>-supported pd-based bimetallic nanorod for CO oxidation. *J. Phys. Chem. C* **2016**, *120*, 5557–5564. [[CrossRef](#)]
10. Liu, B.; Liu, J.; Li, T.; Zhao, Z.; Gong, X.Q.; Chen, Y.; Duan, A.; Jiang, G.; Wei, Y. Interfacial effects of CeO<sub>2</sub>-supported pd nanorod in catalytic CO oxidation: A theoretical study. *J. Phys. Chem. C* **2015**, *119*, 12923–12934. [[CrossRef](#)]
11. Sun, C.; Li, H.; Chen, L. Nanostructured ceria-based materials: Synthesis, properties, and applications. *Energy Environ. Sci.* **2012**, *5*, 8475–8505. [[CrossRef](#)]
12. Qin, Y.Y.; Su, Y.Q. A DFT study on heterogeneous Pt/CeO<sub>2</sub> (110) single atom catalysts for CO oxidation. *ChemCatChem* **2021**, *13*, 3857–3863. [[CrossRef](#)]
13. Farmer, J.A.; Campbell, C.T. Ceria maintains smaller metal catalyst particles by strong metal-support bonding. *Science* **2010**, *329*, 933–936. [[CrossRef](#)] [[PubMed](#)]
14. Ding, K.; Gulec, A.; Johnson, A.M.; Schweitzer, N.M.; Stucky, G.D.; Marks, L.D.; Stair, P.C. Identification of active sites in CO oxidation and water-gas shift over supported Pt catalysts. *Science* **2015**, *350*, 189–192. [[CrossRef](#)] [[PubMed](#)]
15. Gänzler, A.M.; Casapu, M.; Vernoux, P.; Loridant, S.; Aires, F.J.C.S.; Epicier, T.; Betz, B.; Hoyer, R.; Grunwaldt, J.D. Tuning the structure of platinum particles on ceria in situ for enhancing the catalytic performance of exhaust gas catalysts. *Angew. Chem. Int. Ed.* **2017**, *56*, 13078–13082. [[CrossRef](#)]
16. Lu, Y.; Thompson, C.; Kunwar, D.; Datye, A.K.; Karim, A.M. Origin of the high CO oxidation activity on CeO<sub>2</sub> supported Pt nanoparticles: Weaker binding of CO or facile oxygen transfer from the support? *ChemCatChem* **2020**, *12*, 1726–1733. [[CrossRef](#)]
17. Ghosh, P.; Camellone, M.F.; Fabris, S. Fluxionality of Au clusters at ceria surfaces during CO oxidation: Relationships among reactivity, size, cohesion, and surface defects from DFT simulations. *J. Phys. Chem. Lett.* **2013**, *4*, 2256–2263. [[CrossRef](#)]
18. Kim, H.Y.; Henkelman, G. CO oxidation at the interface between doped CeO<sub>2</sub> and supported Au nanoclusters. *J. Phys. Chem. Lett.* **2012**, *3*, 2194–2199. [[CrossRef](#)]
19. Nie, L.; Mei, D.; Xiong, H.; Peng, B.; Ren, Z.; Hernandez, X.I.P.; DeLaRiva, A.; Wang, M.; Engelhard, M.H.; Kovarik, L.; et al. Activation of surface lattice oxygen in single-atom Pt/CeO<sub>2</sub> for low-temperature CO oxidation. *Science* **2017**, *358*, 1419–1423. [[CrossRef](#)]

20. Krcha, M.D.; Mayernick, A.D.; Janik, M.J. Periodic trends of oxygen vacancy formation and C-H bond activation over transition metal-doped CeO<sub>2</sub> (111) surfaces. *J. Catal.* **2012**, *293*, 103–115. [[CrossRef](#)]
21. Dutta, G.; Gupta, A.; Waghmare, U.V.; Hegde, M.S. CO adsorption on ionic Pt, Pd and Cu sites in Ce<sub>1-x</sub>M<sub>x</sub>O<sub>2-δ</sub> (M=Pt<sup>2+</sup>, Pd<sup>2+</sup>, Cu<sup>2+</sup>). *J. Chem. Sci.* **2011**, *123*, 509–516. [[CrossRef](#)]
22. Hu, Z.; Li, B.; Sun, X.Y.; Metiu, H. Chemistry of Doped oxides: The activation of surface oxygen and the chemical compensation effect. *J. Phys. Chem. C* **2011**, *115*, 3065–3074. [[CrossRef](#)]
23. Hu, Z.; Metiu, H. Effect of Dopants on the energy of oxygen-vacancy formation at the surface of ceria: Local or global? *J. Phys. Chem. C* **2011**, *115*, 17898–17909. [[CrossRef](#)]
24. Su, Y.Q.; Zhang, L.; Muravev, V.; Hensen, E.J.M. Lattice oxygen activation in transition metal doped ceria. *Chin. J. Catal.* **2020**, *41*, 977–984. [[CrossRef](#)]
25. Su, Y.Q.; Pilot, I.A.W.; Liu, J.X.; Hensen, E.J.M. Stable Pd-doped ceria structures for CH<sub>4</sub> activation and CO oxidation. *ACS Catal.* **2018**, *8*, 75–80. [[CrossRef](#)]
26. Ren, Z.; Liu, N.; Chen, B.; Li, J.; Mei, D. Nucleation of Cu<sub>n</sub> (n = 1–5) clusters and equilibrium morphology of Cu particles supported on CeO<sub>2</sub> surface: A density functional theory study. *J. Phys. Chem. C* **2018**, *122*, 27402–27411. [[CrossRef](#)]
27. Liu, J.X.; Su, Y.; Pilot, I.A.W.; Hensen, E.J.M. A linear scaling relation for CO oxidation on CeO<sub>2</sub>-supported Pd. *J. Am. Chem. Soc.* **2018**, *140*, 4580–4587. [[CrossRef](#)]
28. Kresse, G.; Furthmüller, J. Efficiency of ab-initio total energy calculations for metals and semiconductors using a plane-wave basis set. *Comput. Mater. Sci.* **1996**, *6*, 15–50. [[CrossRef](#)]
29. Kresse, G.; Furthmüller, J. Efficient iterative schemes for ab initio total-energy calculations using a plane-wave basis set. *Phys. Rev. B* **1996**, *54*, 11169–11186. [[CrossRef](#)]
30. Perdew, J.P.; Burke, K.; Ernzerhof, M. Generalized gradient approximation made simple. *Phys. Rev. Lett.* **1996**, *77*, 3865–3868. [[CrossRef](#)]
31. Blöchl, P.E. Projector augmented-wave method. *Phys. Rev. B* **1994**, *50*, 17953–17979. [[CrossRef](#)]
32. Feng, Y.; Wan, Q.; Xiong, H.; Zhou, S.; Chen, X.; Hernandez, X.I.P.; Wang, Y.; Lin, S.; Datye, A.K.; Guo, H. Correlating DFT calculations with CO oxidation reactivity on Ga-doped Pt/CeO<sub>2</sub> single-atom catalysts. *J. Phys. Chem. C* **2018**, *122*, 22460–22468. [[CrossRef](#)]
33. Ren, Z.; Peng, F.; Chen, B.; Mei, D.; Li, J. A combined experimental and computational study of water-gas shift reaction over rod-shaped Ce<sub>0.75</sub>M<sub>0.25</sub>O<sub>2</sub> (M = Ti, Zr, and Mn) supported Cu catalysts. *Int. J. Hydrog. Energy* **2017**, *42*, 30086–30097. [[CrossRef](#)]
34. Henkelman, G.; Arnaldsson, A.; Jónsson, H. A fast and robust algorithm for Bader decomposition of charge density. *Comput. Mater. Sci.* **2006**, *36*, 354–360. [[CrossRef](#)]
35. Henkelman, G.; Uberuaga, B.P.; Jónsson, H. Climbing image nudged elastic band method for finding saddle points and minimum energy paths. *J. Chem. Phys.* **2000**, *113*, 9901–9904. [[CrossRef](#)]